

Increasing amyloplast size in wheat endosperm through mutation of PARC6 affects starch granule morphology

Lara Esch , Qi Yang Ngai , J. Elaine Barclay , Rose McNelly , Sadiye Hayta , Mark A. Smedley ,
Alison M. Smith  and David Seung 

John Innes Centre, Norwich Research Park, Norwich, NR4 7UH, UK

Summary

Authors for correspondence:

Lara Esch

Email: lara.esch@jic.ac.uk

David Seung

Email: david.seung@jic.ac.uk

Received: 24 April 2023

Accepted: 8 June 2023

New Phytologist (2023) **240**: 224–241

doi: 10.1111/nph.19118

Key words: amyloplast, endosperm, PARC6, plastid division, plastids, starch, starch granule, wheat.

- The determination of starch granule morphology in plants is poorly understood. The amyloplasts of wheat endosperm contain large discoid A-type granules and small spherical B-type granules.
- To study the influence of amyloplast structure on these distinct morphological types, we isolated a mutant in durum wheat (*Triticum turgidum*) defective in the plastid division protein PARC6, which had giant plastids in both leaves and endosperm.
- Endosperm amyloplasts of the mutant contained more A- and B-type granules than those of the wild-type. The mutant had increased A- and B-type granule size in mature grains, and its A-type granules had a highly aberrant, lobed surface. This morphological defect was already evident at early stages of grain development and occurred without alterations in polymer structure and composition. Plant growth and grain size, number and starch content were not affected in the mutants despite the large plastid size. Interestingly, mutation of the PARC6 paralog, ARC6, did not increase plastid or starch granule size. We suggest *Tt*PARC6 can complement disrupted *Tt*ARC6 function by interacting with PDV2, the outer plastid envelope protein that typically interacts with ARC6 to promote plastid division.
- We therefore reveal an important role of amyloplast structure in starch granule morphogenesis in wheat.

Introduction

Amyloplasts are specialised nongreen plastids, mostly found in roots, tubers and seeds, which synthesise starch (Sakamoto *et al.*, 2008; Yun & Kawagoe, 2009; Jarvis & López-Juez, 2013; Sun *et al.*, 2018). Starch is comprised of two glucose polymers, amylose and amylopectin, which together form semicrystalline starch granules. In cereal grains, there is a large interspecies diversity in starch granule morphology and composition. This ranges from simple-type starch granules (e.g. in maize), stemming from a single initiation per amyloplast, to compound-type starch granules (e.g. in rice), where multiple starch granules are initiated simultaneously within one amyloplast (Matsushima *et al.*, 2013; Chen *et al.*, 2021). In wheat endosperm, there is a bimodal starch granule size distribution with large discoid A-type granules (18–20 µm diameter) and small spherical B-type granules (6–7 µm diameter) (Parker, 1985; Bechtel *et al.*, 1990; Howard *et al.*, 2011). Typically, one A-type granule is initiated in the amyloplast early during endosperm development. Smaller B-type granules are initiated later during endosperm development and at least partly within amyloplast stromules, thin tubular extensions of the plastid compartment, filled with stroma and surrounded by the plastid envelope (Parker, 1985; Bechtel *et al.*, 1990; Langeveld *et al.*, 2000; Howard *et al.*, 2011; Hanson & Conklin,

2020). The broad range of starch granule size distributions found in cereal grains strongly influences the end-use quality of starch, for example, by affecting gelatinisation, viscosity and swelling characteristics (Chen *et al.*, 2021).

Recently, advances in the understanding of proteins that influence granule morphology in important staple crops like wheat and barley (Chia *et al.*, 2020; Hawkins *et al.*, 2021; Chen *et al.*, 2022a). Given the occurrence of B-type granules in stromules, amyloplast morphology is also likely to play an important role in the spatial coordination of A- and B-type granule formation (Parker, 1985; Bechtel *et al.*, 1990; Langeveld *et al.*, 2000; Howard *et al.*, 2011; Matsushima & Hisano, 2019). However, the role of amyloplast structure in the initiation and morphogenesis of starch in wheat has not been studied. Investigating the impact of amyloplast structure in wheat could reveal important new insights into the formation of the unique bimodal granule morphology and potentially provide new genetic targets for starch modification.

Plastid size and morphology are greatly influenced by plastid division. The division machinery consists of ring-shaped protein complexes at the inner and outer envelope membranes (Filamenting temperature-sensitive mutant Z (FtsZ) and dynamin rings, respectively), which divide the plastids by binary fission

(Miyagishima, 2011; Yoshida *et al.*, 2012; Osteryoung & Pyke, 2014; Chen *et al.*, 2018; Yoshida & Mogi, 2019). These contractile rings are coordinated by two sets of paralogous proteins that are important for transferring positional information from the FtsZ ring in the plastid stroma to the outside of the plastid, where the dynamin ring is formed (Chen *et al.*, 2018; Yoshida & Mogi, 2019). Accumulation and Replication of Chloroplasts 6 (ARC6), a protein related to the cyanobacterial division protein Ftn2 (Vitha *et al.*, 2003), spans the inner envelope membrane and tethers the FtsZ ring to the inner envelope membrane by interacting with its FtsZ2 subunits (Johnson *et al.*, 2013). In the intermembrane space, the C-terminal domains of two ARC6 molecules interact with those of two Plastid Division 2 (PDV2) proteins to form a heterotetramer (Koksharova & Wolk, 2002; Vitha *et al.*, 2003; Mazouni *et al.*, 2004; Glynn *et al.*, 2008; Marbouty *et al.*, 2009; Wang *et al.*, 2017). Paralog of ARC6 (PARC6) arose from an early duplication of ARC6 in vascular plants (Miyagishima *et al.*, 2006; Glynn *et al.*, 2009). It interacts with FtsZ2 in the chloroplast stroma and C-terminally with Plastid division 1 (PDV1), a protein probably also specific to vascular plants and originating from a duplication of PDV2 (Miyagishima *et al.*, 2006; Glynn *et al.*, 2009; Sun *et al.*, 2023). PDV1 and PDV2 are responsible for recruitment of the Dnm2 (ARC5) subunits that form the outer dynamin ring at the plastid division site (Chen *et al.*, 2018).

This model of plastid division by binary fission is mainly based on studies of *Arabidopsis* mesophyll chloroplasts (Chen *et al.*, 2018), but there is evidence to suggest that the mechanism of division could differ between cell types, organs and species (Mingo-Castel *et al.*, 1991; Bechtel & Wilson, 2003; Ishikawa *et al.*, 2020). For example, *Arabidopsis* *parc6* mutants have giant chloroplasts in mesophyll cells (Glynn *et al.*, 2009), but the effects of the *parc6* mutation on plastid morphology vary between different epidermal cell types (Ishikawa *et al.*, 2020): In pavement cells, the mutant has aberrant grape-like plastid morphology. In trichome cells, plastids exhibit extreme grape-like aggregations, without the production of giant plastids. Finally in guard cells, plastids are reduced in number, enlarged in size and have activated stromules. Amyloplasts may also vary in their division mechanism. Dumbbell-shaped amyloplasts that appeared to undergo binary fission were observed in potato tubers (Mingo-Castel *et al.*, 1991), but not in wheat endosperm, where it was proposed that amyloplasts rather divide through the formation of protrusions (Bechtel & Wilson, 2003). In rice endosperm, amyloplasts were shown to divide simultaneously at multiple sites, forming a beads-on-a-string-like structure (Yun & Kawagoe, 2009).

Due to the differences between species in starch granule initiation patterns in amyloplasts, it is difficult to predict the effect of altered amyloplast size on the initiation and morphogenesis of A- and B-type granules in wheat. Disruption of *ARC6* in *Arabidopsis* greatly increased amyloplast size in root columella cells, and these appeared to contain larger starch granules (Robertson *et al.*, 1995). Mutation of *ARC5* in rice resulted in either fused amyloplasts with thick connections or pleomorphic plastids with multiple division sites, and this was accompanied by an overall reduction in granulae size and potentially granule fusion (Yun &

Kawagoe, 2009). In potato, increased expression of *FtsZ1* resulted in fewer but larger starch granules within the tuber (De Pater *et al.*, 2006). Whether these tubers had larger amyloplasts was not examined, but it is a possibility since in *Arabidopsis*, overexpression of *FtsZ* results in larger amyloplasts (Stokes *et al.*, 2000). As part of the broader goal to understand the relationship between amyloplast structure and starch granule biogenesis, we aimed to examine the role of ARC6 and PARC6 on plastid division in wheat endosperm and their impacts on A- and B-type starch granule initiation and morphogenesis.

Materials and Methods

Plant material and growth conditions

Mutants in *Triticum turgidum* L. (cv Kronos) were selected from the wheat Targeting Induced Local Lesions IN Genomes (TILLING) mutant resource (Krasileva *et al.*, 2017). The *ARC6* and *PARC6* orthologs of wheat were confirmed using phylogenetic tree analysis (Supporting Information Fig. S1; Methods S1). The mutations were genotyped using Kompetitive Allele Specific PCR (KASP) with the KASP v4 master mix (LGC) and the primers in Table S1.

Wheat plants were grown in controlled environment rooms or glasshouses. Controlled environments were set to 16 h : 8 h, light : dark cycles with light intensity set to 300–400 $\mu\text{mol photons m}^{-2} \text{s}^{-1}$. Glasshouses were set to provide a minimum of 16 h light at 300–400 $\mu\text{mol photons m}^{-2} \text{s}^{-1}$. In both cases, temperature was set to 20°C in light and 16°C in the dark, and relative humidity was set to 60%. *Nicotiana benthamiana* plants were grown in the glasshouse set to a minimum of 16 h light at 22°C.

Plant transformation

The *cTPmCherry* construct was generated using Gateway cloning into the pGGG_AH_Ubi_GW_NosT vector backbone, which encodes a Hygromycin resistance gene driven by an actin promoter (AH), a gateway cassette for gateway recombination (GW) downstream of the ZmUbiquitin promoter (Ubi) and upstream of a Nos terminator (NosT) (full details in Methods S2). The construct was transformed into *T. turgidum* cv Kronos using *Agrobacterium*-mediated transformation of embryonic calli, as described in Hayta *et al.* (2021). Lines with single insertions were selected using RT-PCR against the Hygromycin marker gene (performed by iDNA Genetics, Norwich, UK). *Nicotiana benthamiana* leaves were transiently transformed by infiltrating *Agrobacterium* cultures harbouring the appropriate constructs (cloned according to Methods S2 and using the codon-optimised coding sequences in Table S2) into the abaxial side of leaves, as described in Methods S3.

Grain and plant morphometrics

The number of grains harvested per plant, as well as grain size traits (area, length, width, total grain weight per plant and thousand-grain weight), was quantified using the MARViN seed analyser (Marvitech GmbH, Wittenburg, Germany). Grains of three plants per genotype (60–259 individual grains per plant) were analysed. The

number of tillers was counted in mature plants before grain harvesting. Gas-exchange parameters were measured using an LI-6800P (Li-Cor Biosciences, Cambridge, UK), as described in Methods S4.

Starch purification, granule morphology and size distribution

Starch purification, scanning electron microscopy and polarised light microscopy were performed as described in Hawkins *et al.* (2021). Briefly, starch granules were purified from homogenates using filtration and a Percoll cushion. Granule size distribution was analysed and plotted in relative volume/diameter using the Multisizer 4e Coulter Counter (Beckman Coulter, High Wycombe, UK). Morphology of starch granules was examined using a Nova NanoSEM 450 (FEI, Hillsboro, OR, USA) scanning electron microscope and a DM6000 microscope (Leica Microsystems, Milton Keynes, UK) for polarised light microscopy. Full methods are provided in Methods S5.

Total starch content, starch composition, amylopectin structure and Rapid Visco Analysis

Grain starch quantification was performed using a hexokinase/glucose-6-phosphate dehydrogenase-based glucose assay, following the hydrolysis of starch using α -amylase and amyloglucosidase; as described in Hawkins *et al.* (2021) and Methods S6. Full methods for amylopectin chain length distribution and amylose content are in Methods S6 and Chen *et al.* (2022a). Briefly, amylopectin chain length distribution was quantified using high-performance anion exchange chromatography with pulsed amperometric detection (HPAEC-PAD) on a Dionex ICS-5000-PAD fitted with a PA-100 column (Thermo-Fisher Scientific, Loughborough, UK). The preparation of debranched samples was carried out as described in Streb *et al.* (2008). Amylose content was determined using an iodine-binding method (Washington *et al.*, 2000). Rapid Visco Analysis (RVA) was carried out on an RVA Tecmaster instrument (Perten, Waltham, MA, USA) running the preinstalled general pasting method (AACC Method 76-21). Analyses were performed with 1.5 g purified starch or 5 g flour in 25 ml of water.

Protein localisation in *Nicotiana benthamiana*

For localisation of fluorophore-tagged *Ta*PARC6-YFP, *Ta*ARC6-YFP, GFP-*Ta*PDV1-2 and GFP-*Ta*PDV2 in *N. benthamiana*, images were acquired on the Leica Stellaris 8 laser-scanning confocal microscope using a $\times 40.0$ water immersion objective. YFP signal was excited using a white light laser set to 514 nm, and emission was detected at 519–560 nm. GFP signal was excited using a white light laser set to 488 nm and emission was detected at 562–623 nm. Chlorophyll autofluorescence was excited using a white light laser set to 555, 576, or 587 nm and emission was detected at 642–750 nm.

Analysis of plastid morphology

Chloroplasts in fixed mesophyll cells were imaged using confocal microscopy, as described in Methods S7. Amyloplast

morphology in the endosperm was examined as described in Methods S8. Briefly, for transmission electron microscopy, developing grains at 16 day after flowering were fixed and embedded in LR White resin. Ultrathin sections were prepared and imaged on a Talos 200C TEM (FEI) at 200 kV and a OneView 4K \times 4K camera (Gatan, Warrendale, PA, USA). For confocal microscopy, cross sections of live developing endosperm were prepared on a vibratome, mCherry signal was excited at 561 nm, and emission was detected at 562–623 nm (605 nm).

Protein extraction and immunoblotting

For the pairwise immunoprecipitation assays, two 1 cm diameter leaf discs from two *N. benthamiana* leaves transiently expressing the tagged proteins were homogenised in extraction buffer (50 mM Tris-HCl, pH 8.0, 150 mM NaCl, 1% v/v Triton X-100, 1 \times protease inhibitor cocktail, 1 mM DTT). Homogenates were spun at 20 000 g, 10 min, and proteins were collected in the supernatant (Input sample). Immunoprecipitation was performed on the input sample using the μ MACS GFP Isolation Kit (Miltenyi Biotec, Woking, UK) or the RFP-Trap Magnetic Particles (Chromotek, Planegg, Germany) and μ MACS Columns (Miltenyi Biotec). For immunoblotting, antibodies were used in the following concentrations: 1 : 5000 anti-GFP (TP401; Torrey Pines, Biolabs, Secaucus, NJ, USA), 1 : 2000 anti-RFP (ab34771; Abcam, Cambridge, UK) and 1 : 5000 anti-HA (ab9110; Abcam). Bands were detected using the anti-rabbit IgG (whole molecule)-Peroxidase (A0545; Sigma) at 1 : 20 000 dilution and the Super-Signal West Femto Trial Kit (Thermo Scientific).

Results

Identification of *ARC6* and *PARC6* genes in wheat

We first generated mutants in durum wheat (*T. turgidum* ssp. *durum*) defective in *ARC6* and *PARC6*, to test whether they have increased amyloplast size in the endosperm. Using BLASTP against the bread wheat (*Triticum aestivum*) reference genome (Appels *et al.*, 2018), we identified three putative homeologs of *ARC6* encoded on group 6 chromosomes: *Ta*ARC6-A1 (TraesCS6A02G066200.3), *Ta*ARC6-B1 (TraesCS6B02G089500.2), *Ta*ARC6-D1 (TraesCSU02G117700.1) (Figs S1, S2a); as well as three putative homeologs of *PARC6* encoded on group 2 chromosomes: *Ta*PARC6-A1 (TraesCS2A02G555400.1), *Ta*PARC6-B1 (TraesCS2B02G588400.1) and *Ta*PARC6-D1 (TraesCS2D02G559100.1) (Figs 1a, S1). We confirmed these genes as orthologs of Arabidopsis *ARC6* and *PARC6*, respectively, using phylogenetic tree analysis (Fig. S1). In the durum wheat (*T. turgidum* ssp. *durum*) reference genome (Svevo.v1, Maccaferri *et al.*, 2019), the homeologs of *Ta*ARC6 corresponded to *Tt*ARC6-A1 (TRITD6Av1G015630.3) and *Tt*ARC6-B1 (TRITD6Bv1G022070.1), and their predicted amino acid sequences were identical to the bread wheat sequences. *PARC6* in durum wheat corresponded to *Tt*PARC6-A1 (TRITD2Av1G286550.2) and *Tt*PARC6-B1 (TRITD2Bv1G255410.2). The predicted amino acid sequences from these primary gene models were 86.6% and 97.1% identical to their

corresponding homeologs in bread wheat, respectively. Our analysis confirmed that both *ARC6* and *PARC6* genes are highly conserved in plants, and both durum and bread wheat have a single set of homeologs for each gene (Fig. S1).

Phenotypic analysis of *Ttparc6* and *Ttarc6* mutants

To isolate *Ttparc6* and *Ttarc6* mutants, we used the wheat TILLING mutant resource, featuring exome-capture sequenced, EMS-mutagenized mutants of durum cultivar Kronos (Krasileva *et al.*, 2017). We obtained line Kronos1265 (K1265) that carries a premature stop codon in place of Gln503 in *TtPARC6-A1* and Kronos2369 (K2369) carrying a premature stop codon in place of Gln456 in *TtPARC6-B1* (Fig. 1a). The K1265 and K2369 lines were crossed to create the *Ttparc6-1* and *Ttparc6-2* lines, arising from two independent crossing events using separate plants. KASP genotyping was used to identify homozygous single and double mutants for A- and B-genome mutations (*aaBB*, *AAAb* and *aabb*) and the corresponding ‘wild-type segregants’ (*AABB*) in the F2 and F3 generation. We also crossed the *Ttparc6-2* double mutant with a transgenic amyloplast reporter line in cultivar Kronos, to serve two purposes: First, this transgenic line was not exposed to EMS mutagenesis and was therefore a suitable genetic background for backcrossing to remove undesirable background mutations in *Ttparc6-2*. Second, the line carries a single *Maize Ubiquitin (ZmUbi)* promoter-driven transgene encoding an mCherry protein targeted to the plastid stroma with an *OsWaxy* transit peptide, enabling visualisation of amyloplasts (Matsushima & Hisano, 2019; Methods S2). KASP and PCR-based genotyping were used to isolate backcrossed (BC) individuals for each *PARC6* genotype (BC *AABB*, BC *aaBB*, BC *AAAb*, and BC *aabb*), as well as double mutant and wild-type segregant lines carrying the reporter transgene (*Ttparc6-2*+*cTPmCherry aabb* and *Ttparc6-2*+*cTPmCherry AABB*).

Under our growth conditions, the single- or double-mutant lines for *Ttparc6* were identical to their wild-type controls with respect to growth, development and number of tillers (Figs 1b,c, S3a,b,i). To examine whether the mutations affected chloroplast size in leaves, we used confocal microscopy on mesophyll cells isolated from the youngest fully developed leaf of seedlings. Chloroplast size was drastically increased in both backcrossed and nonbackcrossed double mutant lines compared with their wild-type controls (Fig. 1d–h). In the single mutants (*Ttparc6-1* *AAAb*, *Ttparc6-1* *aaBB*, *Ttparc6* BC *AAAb* and *Ttparc6* BC *aaBB*), chloroplast size was visually indistinguishable from the wild-type controls (Fig. S3c–j).

Since the *Ttparc6* double mutants had increased chloroplast size but seemingly normal growth, we examined their photosynthetic efficiency using gas-exchange analysis (Fig. S4). In light response curves, both the backcrossed and nonbackcrossed double mutants showed a slight tendency towards decreased photosynthesis rates (*A*) compared with the wild-type controls (Fig. S4a–e), but statistical analysis of extracted *A* values at ambient ($280 \mu\text{mol m}^{-2} \text{s}^{-1}$) or high light ($2000 \mu\text{mol m}^{-2} \text{s}^{-1}$) revealed no differences between the mutants and wild-type controls (Fig. S4f). There were also no significant differences between the mutants and wild-type controls

in maximal carboxylation rate (V_{cmax} ; Fig. S4g). Although the maximal electron transport (J_{max}) was significantly decreased in the backcrossed double mutant (*Ttparc6* BC *aabb*) compared with its backcrossed wild-type segregant (*Ttparc6* BC *AABB*), it was not significant when compared with the wild-type. The J_{max} of the nonbackcrossed *Ttparc6-1 aabb* double mutant was also not different to its wild-type controls (Fig. S4h). Therefore, we did not detect any consistent effect of the *Ttparc6* mutations on the measured photosynthetic parameters.

Using an approach similar to that for *TtPARC6*, we also isolated a mutant defective in both homeologs of *TtARC6*, crossing the lines Kronos3404 (K3404) and Kronos2205 (K2205) to introduce premature stop codons in place of Gln631 in *TtARC6-A1* and in place of Trp647 in *TtARC6-B1* (Fig. S2a). Unlike both wheat *Ttparc6* mutants described above and Arabidopsis *arc6* mutants (Vitha *et al.*, 2003), chloroplast size was unaffected by the *Ttarc6* mutations (Fig. S2b,c). Therefore, we focused our analyses of endosperm starch on the *Ttparc6* mutants.

Ttparc6 mutants have normal grain size, number and yield

We examined the grains harvested from the *Ttparc6* mutants (Figs 2a,b, S3k). The total grain yield per plant for the backcrossed and nonbackcrossed double mutants, as well as for the single mutants, was not significantly different from their wild-type controls (Figs 2c, S3m). There was also no consistent effect of *Ttparc6* mutations on grain size, weight and total starch content (Figs 2d, S3o,p). The average thousand-grain weight (TGW) for the nonbackcrossed *Ttparc6* double and single mutants was not significantly different to the wild-type controls (Figs 2d, S3n). However, the TGW of the backcrossed *Ttparc6* BC *aabb* double mutant was significantly higher than in the wild-type controls (24% increase relative to the WT) (Fig. 2d). Grain size parameters were also significantly higher in this backcrossed double mutant than in the wild-type segregant and the WT (area, width and length increased by 15%, 10% and 6%, respectively) (Fig. 2f–h). Since these increases in grain weight and size were only observed in the backcrossed double mutants and not in the nonbackcrossed double mutant, they are either not caused directly by the *Ttparc6* mutations, or other mutations in the nonbackcrossed lines suppress the increased grain size.

Ttparc6 mutants have increased starch granule sizes in the endosperm

We purified starch granules from mature grains of the *Ttparc6* mutants and examined starch granule size and morphology. Using a Coulter Counter, we observed that all genotypes had a bimodal distribution of starch granule size (Fig. 3a,b). In the wild-type, the A-type granule peak had its maximum at *c.* 19 μm diameter and the B-type granule peak maximum was at *c.* 6 μm diameter.

The *Ttparc6* double mutants had drastically altered granule size distributions compared with the WT and the corresponding wild-type segregants. The A-type granule peak in the mutants was shifted towards larger granule diameters (*c.* 22–24 μm diameter); the B-type granule peak was not only shifted to larger

granule sizes (c. 8–9.5 μm diameter) but also had a larger peak area. We fitted a log-normal distribution to the B-type granule peak and a normal distribution to the A-type granule peak to derive the mean diameters of A- and B-type granules, as well as the B-type granule content (percentage of total starch volume

that is present as B-type granules). The mean diameter of A-type granules of both double-mutant (*aabb*) genotypes were significantly larger than those of their corresponding wild-type controls (15.1% increase in *Ttparc6-1 aabb* and 21.9% increase in *Ttparc6 BC aabb*) (Fig. 3c). While there was a shift towards

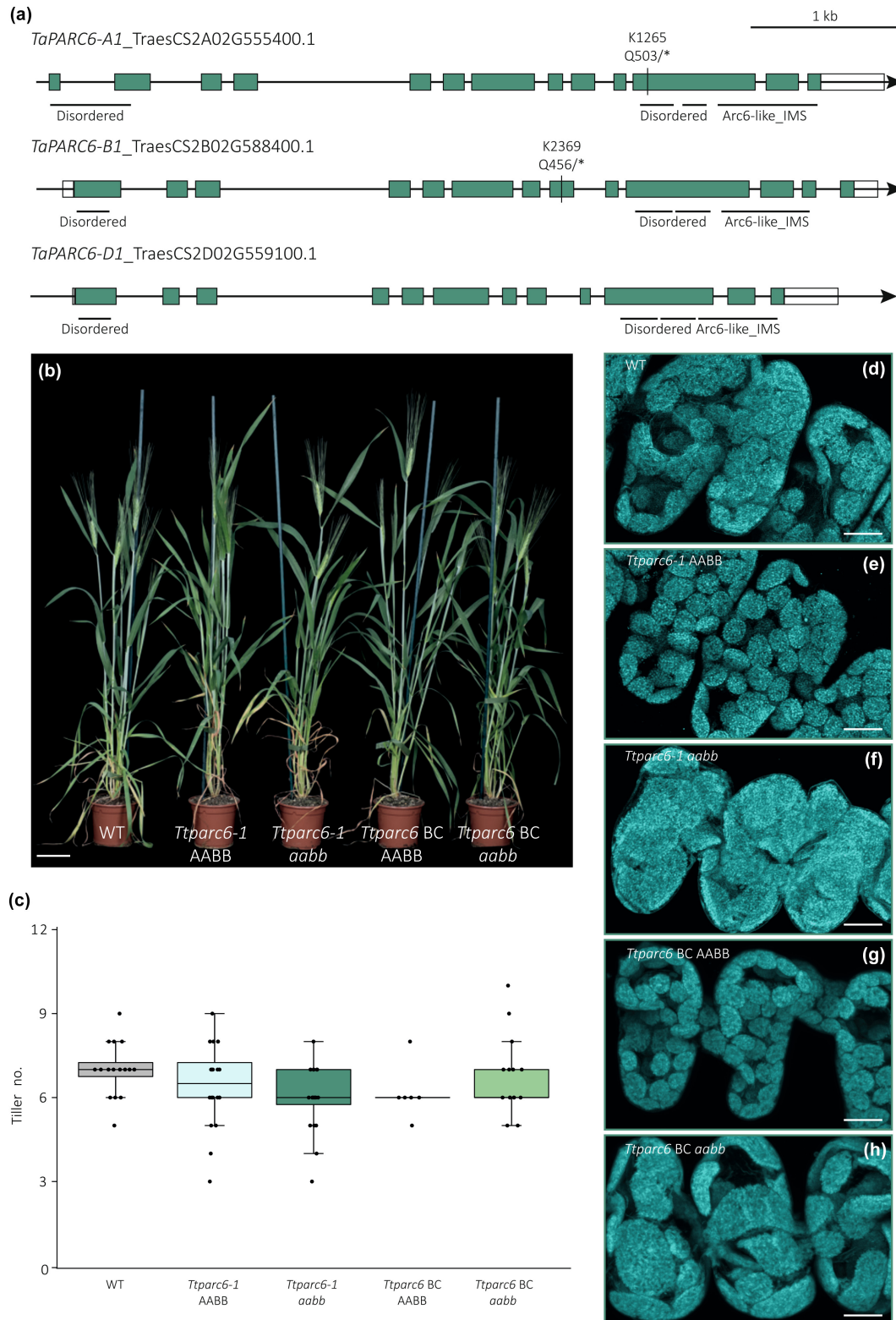


Fig. 1 Growth phenotype of *Ttparc6* durum wheat mutants. (a) Schematic illustration of the gene models for the primary transcripts of *TaPARC6-A1*, *TaPARC6-B1* and *TaPARC6-D1* in bread wheat. Exons are represented as teal boxes and untranslated regions (UTRs) are represented as white boxes. Mutation sites in K1265 and K2369 are indicated by black lines and the resulting amino acid to stop codon (*) substitutions are annotated. Regions encoding domains are indicated by black horizontal lines (IMS, intermembrane space). (b) Photograph of 8-wk-old *Ttparc6* double mutant (*Ttparc6-1 aabb*), the corresponding wild-type (WT) segregant (*Ttparc6-1 AABB*), *Ttparc6* backcrossed double mutant (*Ttparc6 BC aabb*), the corresponding WT segregant (*Ttparc6 BC AABB*) and WT wheat (cv Kronos) plants. Bar, 10 cm. (c) The number of tillers per plant (Tiller no.) of mature *Ttparc6* mutant plants. The top and the bottom of the box represent the lower and upper quartiles, respectively, and the band inside the box represents the median. The ends of the whiskers represent values within 1.5× of the interquartile range. Outliers are values outside 1.5× the interquartile range. There is no significant difference between the lines as determined by Kruskal–Wallis one-way analysis of variance (ANOVA) on ranks: $P = 0.097$. (d–h) Images of mesophyll-cell chloroplasts in the third leaf of *Ttparc6* mutant seedlings. Images were acquired using confocal microscopy and are Z-projections of image stacks. Chlorophyll autofluorescence of the chloroplasts is shown in cyan. Bar, 10 μm.

larger B-type granule sizes in both the *Ttparc6-1 aabb* double mutants, only the backcrossed double mutant genotype had a significant increase in the mean diameter of B-type granules (27.3% increase in *Ttparc6-1 aabb* and 43.5% increase in *Ttparc6 BC aabb*) (Fig. 3d). However, we detected a large, significant increase in B-type granule content in both *Ttparc6-1 aabb* and *Ttparc6 BC aabb* double mutants, that ranged from 67% to 73% in double mutant genotypes vs 35% to 45% in WT and their wild-type segregants (Fig. 3e). There were no significant differences in the numbers of starch granules present (per mg of starch) between the *Ttparc6* double mutants and the controls (Fig. 3f).

Interestingly, we also observed a striking dosage effect of *Ttparc6* mutations on the granule size distribution. The *Ttparc6* single homeolog mutants had an intermediate change in granule size distribution, and the associated size parameters (A-type granule diameter, B-type granule diameter and B-type granule content) were in between those of the double mutants and the wild-type segregants (Fig. S5a–h).

We then examined starch granule morphology of the purified starches using the scanning electron microscope (SEM). Consistent with the results from the size quantification using the Coulter Counter, we observed extremely large A-type granules. Surprisingly, most of the A-type granules in the double mutants had a distinct lobate, crumpled appearance (Fig. 3g–k). Using polarised light microscopy, most of the very large A-type granules had a disrupted Maltese cross, and some had no cross (Fig. 3l–p). A similar lobed surface structure and altered birefringence were observed in A-type granules of the single homeolog mutants (Fig. S5i–r).

Granule morphology is altered throughout grain development in *Ttparc6* mutants

To determine how the alterations in granule size and morphology arise in the *Ttparc6* mutants, we examined granules of the *Ttparc6-2* double mutant in developing grains at 12, 16 and 21 day after flowering (DAF; Figs 4, 5). At 12 DAF, before the initiation of B-type starch granules, the A-type granules of the *Ttparc6-2 aabb* mutant were similar in size to those of the wild-type (mean diameter of 14.4 and 14.0 μm respectively) (Figs 4a, 5a). However, even at this time point, the double mutant already had strong alterations in A-type granule morphology, which were similar to those observed in the mature grain (Fig. 4e,f,m,n). The synthesis of B-type granules had initiated by 16 DAF. By this time point, the A-type granules were significantly larger in diameter than the wild-

type (5% increase) and B-type granule content was also larger than that of the wild-type (98% increase; Figs 4b, 5c). A-type granules in the double mutant remained distinctly lobate, while B-type granules were round and similar to the wild-type (Fig. 4g,h,o,p). The differences in A-type granule diameter, B-type granule diameter and B-type granule content in the *Ttparc6-2 aabb* mutant compared with the wild-type controls increased as grain development progressed (Figs 4c,d, 5). The mature grains of the double mutant had a similar granule size distribution to those observed in the experiments of Figs 4(d,k,l,s,t) and 5.

Ttparc6 double mutants have enlarged amyloplasts that contain multiple starch granules

To assess the effects of the *Ttparc6* mutation on endosperm amyloplasts, we examined sections of developing WT and *Ttparc6-2 aabb* grain at 16 DAF using transmission electron microscopy (TEM; Methods S8). In the wild-type, the amyloplast envelope was tightly associated with the large A-type granules (Fig. 6a,b). We did not see protrusions containing additional granules (A- or B-type granules). However, we observed examples of multiple small B-type granules enclosed within a single amyloplast envelope (Fig. 6c). We found amyloplast size in the *Ttparc6-2 aabb* mutant was increased compared with the WT (Fig. 6d,e). There were single amyloplast compartments containing multiple A- and B-type granules (Fig. 6e). Even in amyloplasts where only a single A-type granule could be observed, the amyloplast envelope was less closely associated with the starch granules than in the wild-type (Fig. 6d). As observed in the wild-type, some amyloplasts in the mutant appeared to contain multiple B-type granules (Fig. 6f).

In addition, we used confocal microscopy to examine amyloplasts in segregants of the *Ttparc6-2 aabb* double mutant carrying a fluorescent amyloplast reporter transgene (as mentioned in the previous section). We imaged cross-sections of the *Ttparc6-2 + cTPmCherry aabb* double mutants and the *Ttparc6-2 + cTPmCherry AABB* wild-type segregant at 16 DAF (Methods S8). Amyloplast size was drastically increased in the double mutant compared with the wild-type segregant, and many amyloplasts in the mutant contained more than one large A-type granule (Fig. 6). Within these amyloplasts the A-type granules appeared to be separated by stromal space (Fig. 6i,j). Amyloplasts in the wild-type segregant were not observed to contain more than one A-type granule (Fig. 6g,h). Consistent with the TEM

images, however, there were multiple B-type granules within one vesicle-like amyloplast compartment in both wild-type and mutant (Fig. 6g–j). We verified that the overexpression of cTPmCherry did not influence the *Ttparc6 aabb* phenotype, by confirming that plant growth, grain size, starch content and granule size distribution were comparable between the lines with and without the reporter (Fig. S6).

Composition of starch of the *Ttparc6* double mutants is similar to wild-type durum wheat starch

We tested whether the highly altered starch granule morphology of the *Ttparc6* mutants resulted from changes in the starch polymer structure and composition. Although increased amylose content relative to the wild-type was observed in both the backcrossed and

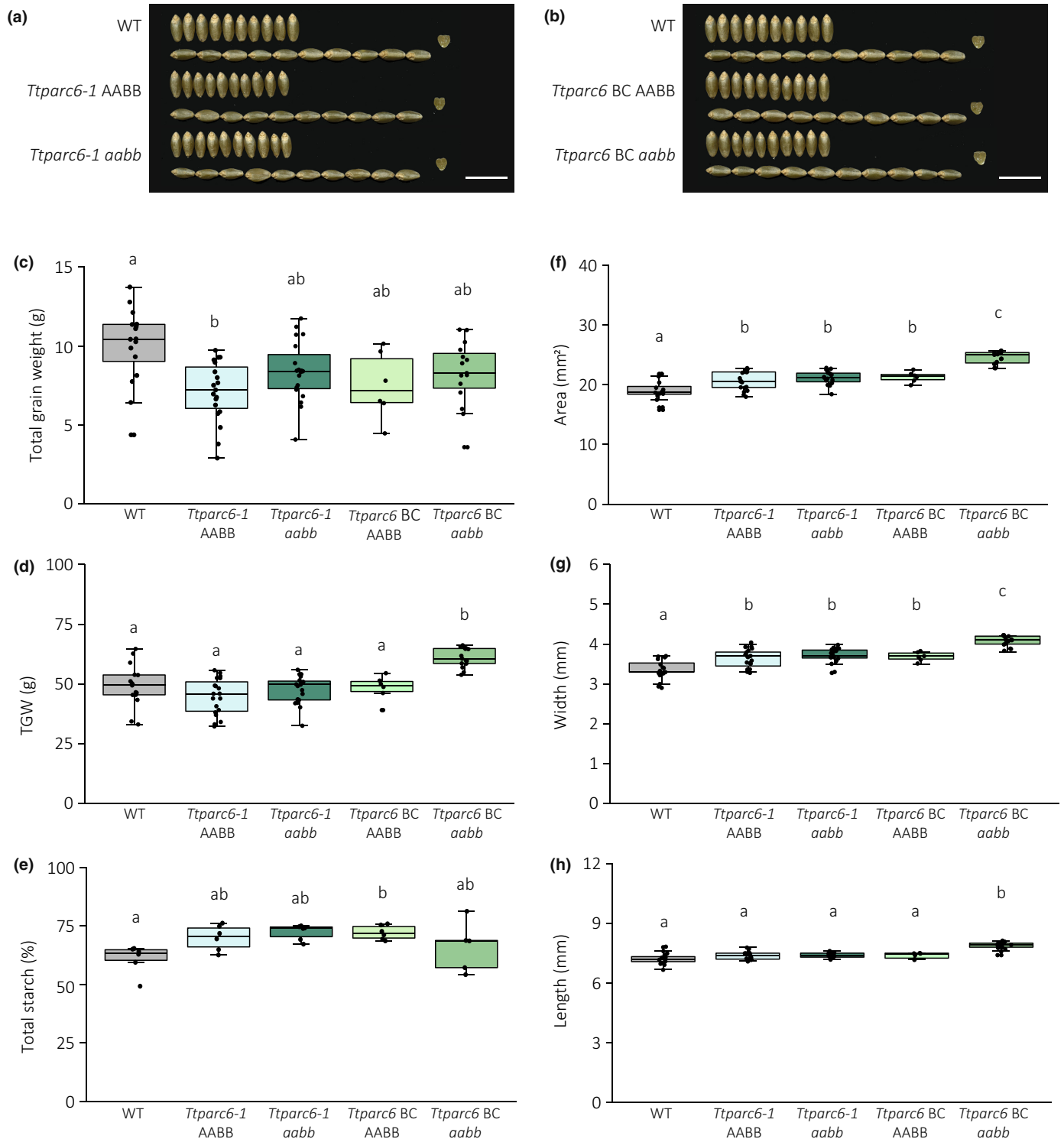


Fig. 2 Seed phenotype of *Ttparc6* durum wheat mutants. (a, b) Photographs of 10 representative mature grains per genotype. Note that the same wild-type (WT) grains were used in both panels. Bar, 1 cm. (c) Total grain weight harvested per plant (in g). Dots represent the total grain weight of individual plants ($n = 6-19$) per genotype. Significant differences under a one-way analysis of variance (ANOVA), and all pairwise multiple comparison procedures (Tukey's test) are indicated with different letters ($P \leq 0.002$). (d) Thousand-grain weight (TGW) (in g). Dots represent calculated TGW of individual plants ($n = 6-19$) per genotype. Significant differences under a one-way ANOVA, and all pairwise multiple comparison procedures (Tukey's test) are indicated with different letters ($P \leq 0.001$). (e) Total starch content as % (w/w). Three technical replicates of two biological replicates per genotype. Significant difference between the genotypes under a Kruskal–Wallis one-way ANOVA on ranks and all pairwise multiple comparison procedures (Tukey's test) are indicated with different letters ($P \leq 0.041$). (f–h) Grain size parameters measured as seed area (f), width (g) and length (h). Dots represent the average for each parameter calculated from grains from individual plants ($n = 6-19$) per genotype. Significant differences under a one-way ANOVA (f, g) or a Kruskal–Wallis one-way ANOVA on ranks (h), and all pairwise multiple comparison procedures (Tukey's test) are indicated with different letters ($P \leq 0.001$). For all box-plots, the bottom and top of the box represent the lower and upper quartiles, respectively, and the band inside the box represents the median. The ends of the whiskers represent values within $1.5 \times$ of the interquartile range, whereas values outside are outliers.

nonbackcrossed double mutants and some of the single mutants (Figs S3q, S7a), the differences in the double mutants were not significant when compared with the wild-type segregant controls and are therefore unlikely to result from *Ttparc6* mutations. The chain length distribution of amylopectin in the *Ttparc6* double mutants was indistinguishable from that of the wild-type and the corresponding wild-type segregants (Fig. S7b). Furthermore, Rapid Visco Analysis (RVA) revealed no consistent difference in viscosity or gelatinisation properties – suggesting that the crystalline structure of the starch granules was unlikely to be altered in the mutant, since changes in crystallinity are usually associated with altered gelatinisation temperature (Fig. S7c,d). In conclusion, the altered starch granule morphology is unlikely to arise from differences in starch composition or polymer structure.

TaPARC6 interacts with both PDV1 and PDV2 paralogs

In contrast to the *Ttparc6* mutant, the *Ttarc6* double mutant did not show increased chloroplast size in the leaves (Fig. S2). The endosperm starch granule size distribution of the *Ttarc6* double mutant (*Ttarc6 aabb*) was also similar to the wild-type segregant (*Ttarc6 AABB*; Fig. S8a). This raised the possibility that the mechanism of plastid division is different in wheat from that in Arabidopsis, in that *arc6* mutations do not have a strong effect. Alternatively, the position of premature stop mutations in our wheat *Ttarc6* mutants (in both A and B homeologs; Fig. S2) might allow the production of a truncated protein with residual function. However, alignment of the amino acid sequences of *TtARC6* and the Arabidopsis *AtARC6* showed that any putative truncated protein in the *Ttarc6* lines would be terminated at a position that is similar to a previously characterised truncated *AtARC6* protein (*Atarc6ΔIMS*), missing the C-terminal intermembrane space region (Glynn *et al.*, 2008; Fig. S9a). In Arabidopsis, this truncation greatly impairs *ARC6* function as it removes the C-terminal interaction site of *AtARC6* with *AtPDV2* and consequently disrupts plastid division (Glynn *et al.*, 2008). We therefore analysed whether the wheat *ARC6* and *PARC6* proteins are capable of interacting with the wheat *PDV2* and *PDV1* orthologs, respectively, as observed previously for the homologous proteins in Arabidopsis. We identified the corresponding wheat orthologs of *PDV1* and *PDV2* using BLAST and phylogenetic tree analysis (Fig. S9b). In vascular plants, an early duplication gave rise to both *PDV1* and *PDV2*, proteins. Interestingly, within the Pooidae, there was an additional duplication

of *PDV1* (resulting in *PDV1-1* and *PDV1-2*) also hinting possible differences in the plastid division mechanism in wheat compared with Arabidopsis (Fig. S9b).

We cloned the A-genome homeologs of wheat *ARC6*, *PARC6*, *PDV1-1*, *PDV1-2* and *PDV2*. *TaPARC6* and *TaARC6* that were C-terminally tagged with a yellow fluorescent protein (YFP) and transiently expressed in *N. benthamiana* under control of an Arabidopsis Ubiquitin 10 promoter and a Cauliflower Mosaic Virus (CaMV) 35S promoter, respectively (Methods S2). Using confocal microscopy, we observed that *TaPARC6-A1-YFP* localised to distinct puncta in the plastid in pavement cells (Fig. 7a–c). These puncta localised more towards the periphery of the chloroplast and did not colocalise with the chlorophyll autofluorescence, indicating they might be at the chloroplast envelope (Fig. 7a–c). *TaARC6-A1-YFP* was also observed at the chloroplast periphery, but did not form puncta (Fig. 7d–f). *TaPDV1-1-A1*, *TaPDV1-2-A1* and *TaPDV2-A1* are outer envelope proteins and are targeted towards the chloroplasts and anchored in the outer membrane by a C-terminal sequence rather than an N-terminal transit peptide. Thus, we tagged *TaPDV1-1-A1*, *TaPDV1-2-A1* and *TaPDV2-A1* with an N-terminal green fluorescent protein (GFP). We were unable to localise GFP-*TaPDV1-1-A1* when transiently expressed in *N. benthamiana* under control of a CaMV 35S promoter due to low signal intensity. However, GFP-*TaPDV1-2-A1* clearly localised to the chloroplasts, although fluorescence intensity was weak (Fig. 7g–i). GFP-*TaPDV2-A1* localised around the chlorophyll fluorescence, indicating a possible localisation to the chloroplast envelope.

In co-immunoprecipitation experiments, *TaPARC6-GFP* interacted with RFP-*TaPDV1-1* and also weakly with RFP-*TaPDV1-2* and RFP-*TaPDV2* (Fig. 7m). However, *TaARC6-HA* only interacted with GFP-*TaPDV2* (Fig. 7n), as was previously shown for Arabidopsis (Wang *et al.*, 2017). Therefore, it is possible that in wheat, *TaPARC6* might be able to compensate for the loss of *TaARC6* function, by interacting with *PDV2* in addition to *PDV1-1* and *PDV1-2*.

Discussion

Mutation of *TtPARC6* increases amyloplast size and alters starch granule morphology in durum wheat endosperm

Here, we demonstrated that amyloplast architecture is an important factor that determines starch granule morphology. There are

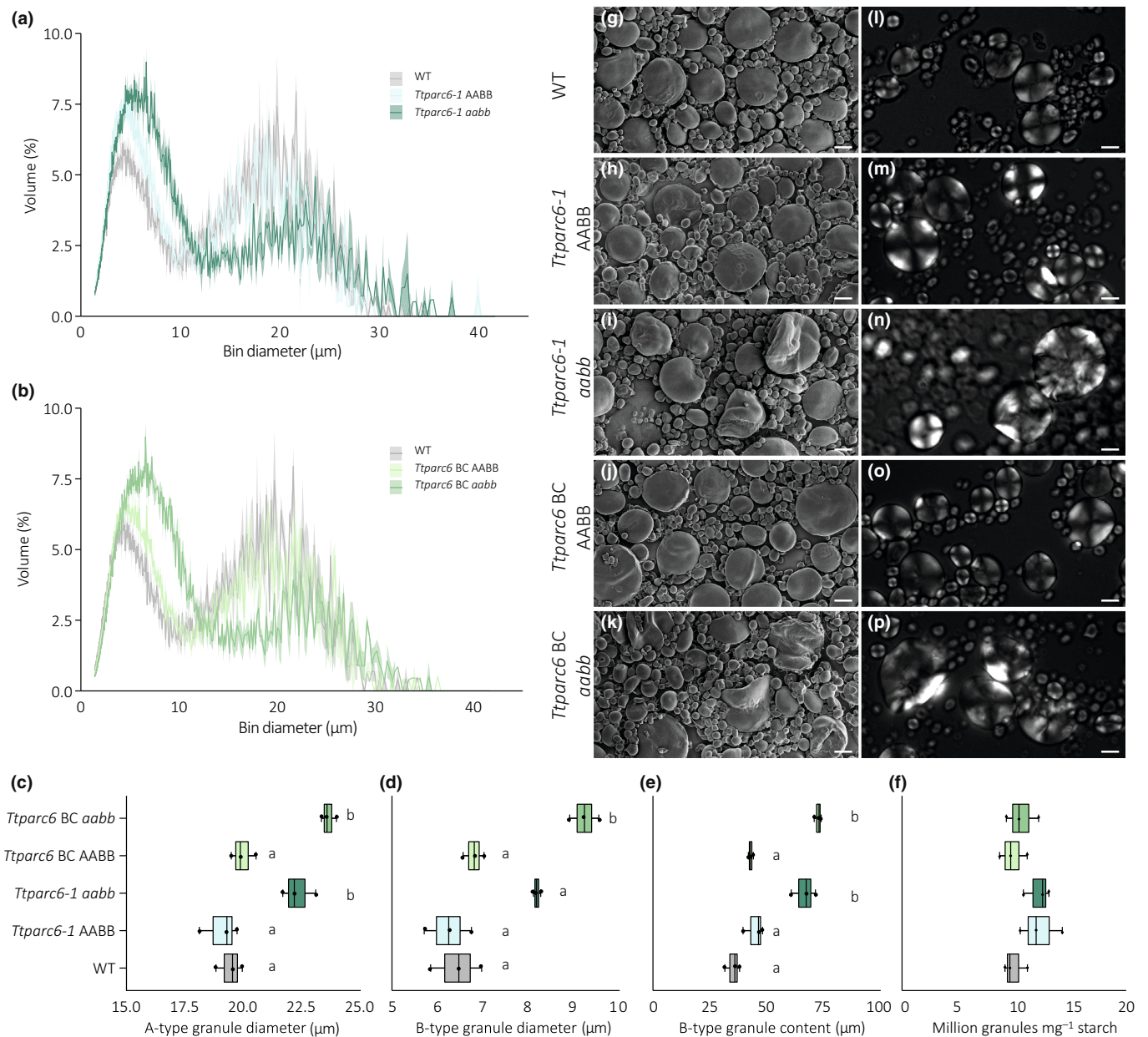


Fig. 3 Size distribution and morphology of purified starch granules from mature grains of *Ttparc6* durum wheat mutants. (a, b) Size distribution plots from Coulter counter analysis. The volume of granules at each diameter relative to the total granule volume was quantified using a Coulter Counter. Values represent mean (solid line) \pm SE (shading) of three replicates using grains harvested from separate plants. (c–e) Granule size parameters obtained from fitting a log-normal distribution to the B-type granule peak and a normal distribution to the A-type granule peak in the granule size distribution data presented in (a, b). Three biological replicates were analysed: (c) A-type granule diameter (in μm). Significant differences under a one-way analysis of variance (ANOVA) and all pairwise multiple comparison procedures (Tukey's test) are indicated with different letters ($P \leq 0.05$). (d) B-type granule diameter (in μm). Significant differences under a Kruskal–Wallis one-way ANOVA on the ranks are indicated with different letters ($P \leq 0.019$). (e) B-type granule content by percentage volume. Significant differences under a one-way ANOVA and all pairwise multiple comparison procedures (Tukey's test) are indicated with different letters ($P \leq 0.019$). (f) Granule number per milligram (mg) starch quantified on the Coulter Counter. There was no significant difference between genotypes under a one-way ANOVA. For all box plots, the left and the right of the box represent the lower and upper quartiles, respectively, and the band inside the box represents the median. The ends of the whiskers represent values within $1.5\times$ of the interquartile range. Outliers are values outside $1.5\times$ the interquartile range. (g–k) Scanning electron microscopy of starch granules from mature grain. Bar, $10\ \mu\text{m}$. (l–p) Polarised light microscopy of starch granules from mature grain. Bar, $10\ \mu\text{m}$. WT, wild-type.

numerous examples of altered granule morphology in wheat arising as a consequence of mutations in genes that affect starch polymer biosynthesis and structure (e.g. SS3 and SBE2) or granule initiation patterns (SS4, BGC1 and MRC) (Carcioli *et al.*, 2012; Chia *et al.*, 2020; Hawkins *et al.*, 2021; Chen *et al.*, 2022a; Fahy

et al., 2022). However, we achieved highly modified granule morphology after mutating a component of plastid division. Our durum wheat mutants defective in *TTPARC6* not only had increased chloroplast size in leaves but also increased amyloplast size in developing endosperm (Figs 1d–h, 6). This was

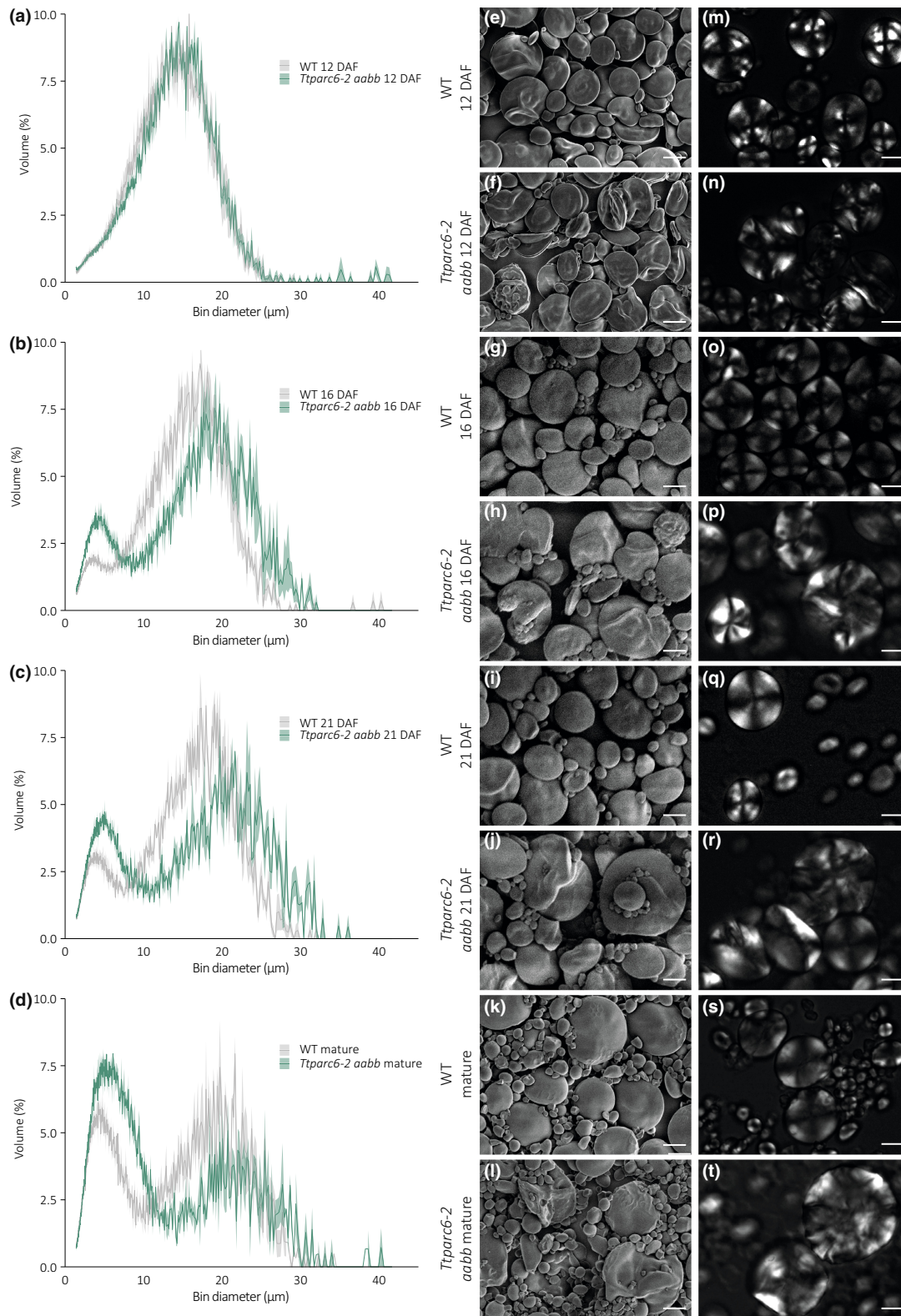


Fig. 4 Size distribution and morphology of purified starch granules from developing grains of *Ttparc6-2* durum wheat mutants. (a–d) Size distribution of purified starch granules from developing (12, 16, 21 day after flowering – DAF) and mature grain. The volume of granules at each diameter relative to the total granule volume was quantified using a Coulter counter. Values represent mean (solid line) ± SEM (shading) of three biological replicates using grains harvested from separate plants. (e–l) Scanning electron microscopy of purified starch granules. Bar, 10 μm. (m–t) Polarised light images of purified starch granules. Bar, 10 μm. WT, wild-type.

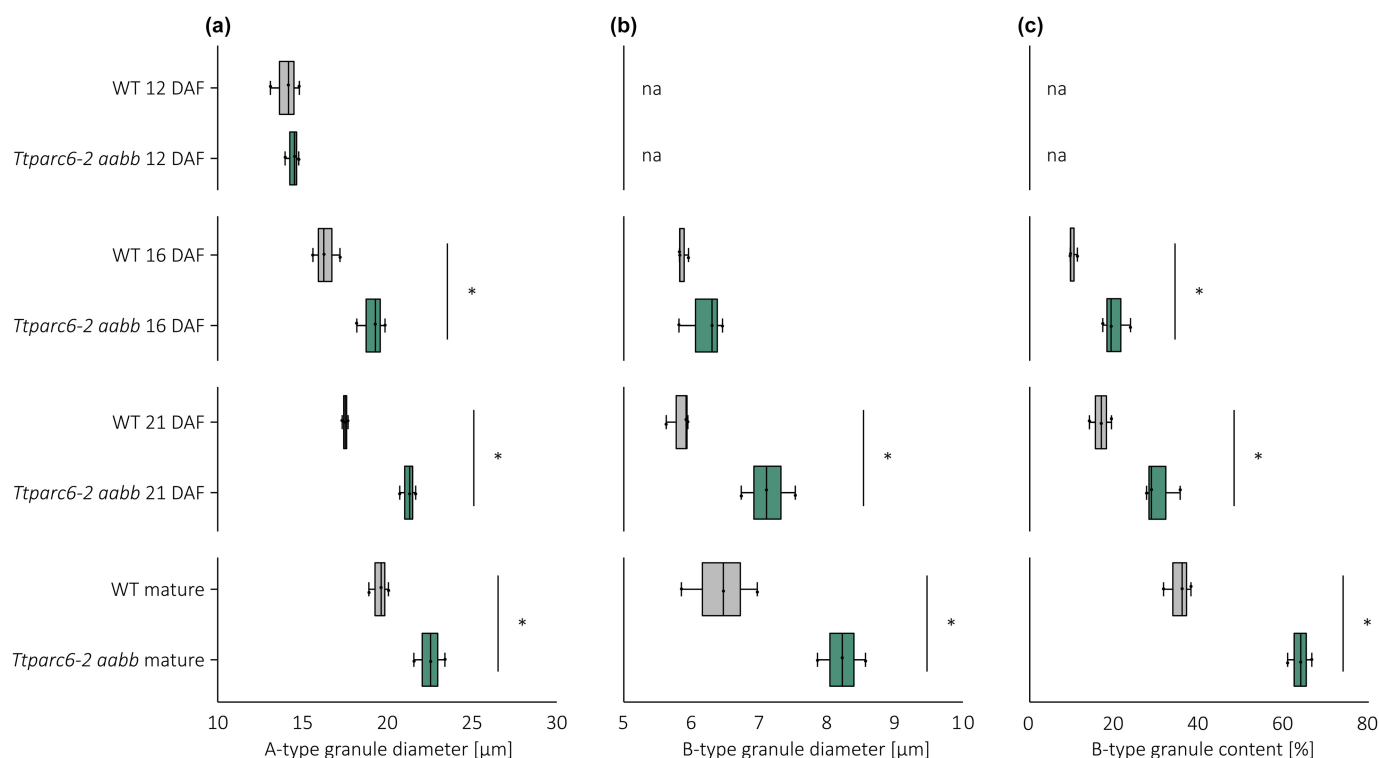


Fig. 5 Starch granule size parameters and B-type granule content of developing *Ttparc6-2* durum wheat grains. (a–c) Granule size parameters obtained from fitting a log-normal distribution to the B-type granule peak and a normal distribution to the A-type granule peak in the granule size distribution data presented in Fig. 4. Only A-type granule peaks could be fitted to the distributions at 12 day after flowering (DAF). Three biological replicates from grains harvested from separate plants were analysed, and significant differences ($P < 0.05$) under a pairwise *t*-test between genotypes at each time point are represented by an asterisk. (a) A-type granule diameter (in μm). (b) B-type granule diameter (in μm). (c) B-type granule content by percentage volume. For all box plots, the left and the right of the box represent the lower and upper quartiles, respectively, and the band inside the box represents the median. The ends of the whiskers represent values within $1.5 \times$ of the interquartile range. Outliers are values outside $1.5 \times$ the interquartile range. Not applicable parameters are indicated by na. WT, wild-type.

accompanied by increased size of both A- and B-type granules in amyloplasts. It is possible that the increases in amyloplast size and accessible stromal volume in the mutant relative to the wild-type may facilitate the formation of larger starch granules. Increased granule size in the mutant relative to the wild-type was noticeable at 16 DAF, shortly after the initiation of B-type granules, while at 12 DAF, starch granule size in the *Ttparc6* double mutant was still similar to the wild-type (Figs 4, 5). Perhaps in early endosperm development, granule size in the wild-type is not yet limited by the available space in the amyloplast while at later stages, amyloplast size potentially becomes a limiting factor.

In addition to the increased starch granule size, we observed that the A-type granules of the *Ttparc6* double mutants had drastically altered, lobate granule morphology, compared with the smooth-surfaced disc shape in the wild-type (Fig. 3). This altered morphology manifested early during grain development (12 DAF), even when the granules of the mutant had the same diameter as those of the wild-type (Fig. 4). The morphogenesis of wild-type A-type granules during endosperm development was studied in detail by Evers (1971), who reported that A-type granules are initially round and then a grooved annular concretion surrounds two-thirds of the granule in an equatorial plane, eventually surrounding the spherical granule as a flange-like

outgrowth to form the disc-shaped A-type granule (Evers, 1971). It is possible that in the *Ttparc6* mutants, this organised morphogenesis of A-type granule formation is at least partially disrupted. Since amylose content and amylopectin structure were not altered in the *Ttparc6* mutants however (Figs S3q, S7a,b), the aberrant size and shape of these granules cannot be caused by differences in starch polymer properties. The granules of the mutant also had similar gelatinisation properties (Fig. S7c,d), indicating that crystalline structure is not likely to be altered. Therefore, the disrupted maltose crosses on the A-type starch granules in polarised light are likely caused by increased refraction on the lobate granule surface rather than changes in starch granule crystallinity (Figs 3k–o, 4m–t). It seems plausible that the enlarged stromal volumes in the *Ttparc6* mutant amyloplasts not only accommodate increased starch granule size, but also influence the usually organised formation of proper A-type granule shape (Fig. 8). Whether this might be due to altered spatial patterns of starch granule growth during granule formation in enlarged plastid compartments remains to be investigated. We recently demonstrated that disrupting the morphology of stromal pockets between the thylakoid membranes in which starch granules form leads to altered granule size and surface structure (Esch *et al.*, 2022), and similar changes in the stromal compartments in

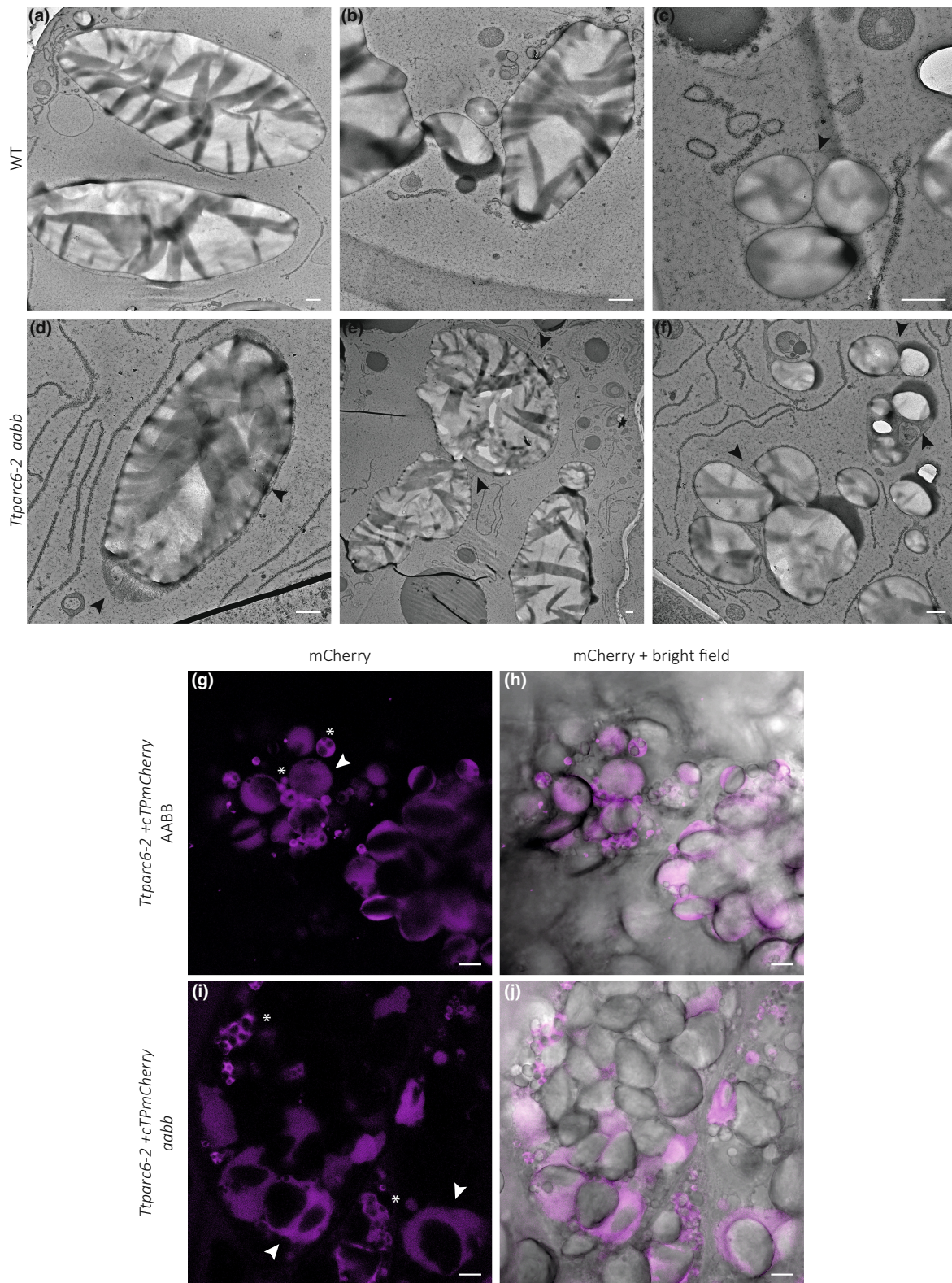


Fig. 6 Amyloplast structure of developing grains of the *Ttparc6* durum wheat mutant. (a–f) Transmission electron microscopy (TEM) images of endosperm sections of developing grain at 16 day after flowering (DAF). Arrows indicate amyloplast membrane. Bar, 1 μm. (g–j) Confocal laser scanning imaging of endosperm sections of developing grain at 16 DAF, in lines stably overexpressing the amyloplast marker *cTPmCherry* shown in magenta. Arrows indicate amyloplasts containing A-type starch granules, whereas asterisks point to clusters of B-type starch granules. Bar, 10 μm. WT, wild-type.

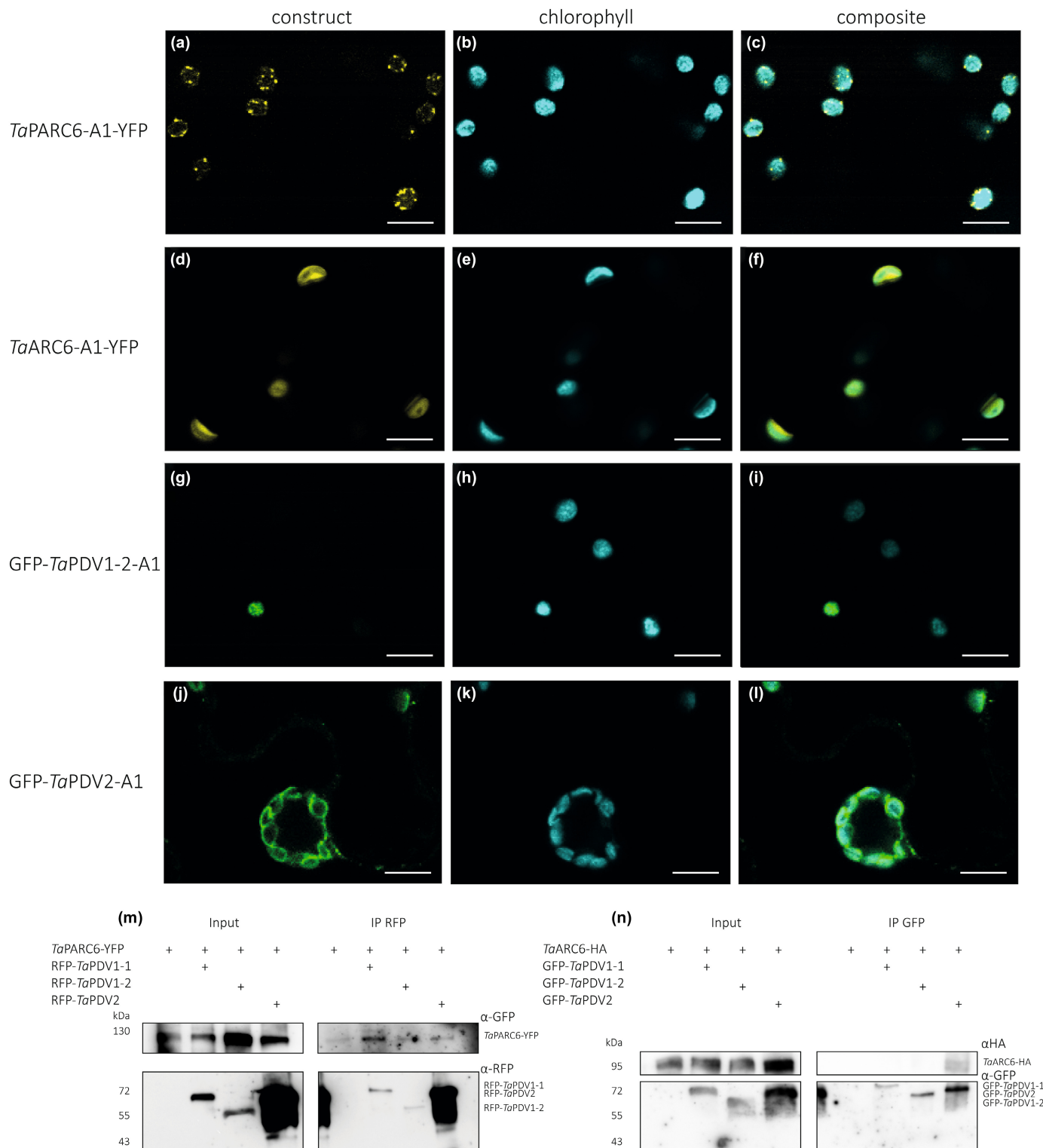


Fig. 7 Localisation and co-immunoprecipitation assays of wheat *TaPARC6*, *TaARC6* and *TaPDV* isoforms. (a–l) Images of transiently expressed *AtUbi::TaPARC6-A1-YFP*, *CaMV35S::TaARC6-A1-YFP*, *CaMV35S::GFP-TaPDV1-2-A1* and *CaMV35S::GFP-TaPDV2-A1* in *Nicotiana benthamiana* epidermal cells. Images were acquired using confocal laser scanning microscopy. The yellow fluorescent protein (YFP) and green fluorescent protein (GFP) fluorescence are shown in yellow and green, while chlorophyll autofluorescence is shown in cyan. Bar, 10 μ m. (m) Immunoprecipitation (IP) assay using anti-red fluorescent protein (RFP) beads for interactions between *TaPARC6-YFP* and RFP-*TaPDV1-1*, RFP-*TaPDV1-2* and RFP-*TaPDV2*, transiently co-expressed in *Nicotiana* leaves. Immunoblots RFP and GFP antibodies were used to detect the proteins. (n) Immunoprecipitation (IP) assay using anti-GFP beads for *TaARC6-HA* and GFP-*TaPDV1-1*, GFP-*TaPDV1-2* and GFP-*TaPDV2*, transiently co-expressed in *Nicotiana* leaves. Immunoblots with HA (hemagglutinin)-tag and GFP antibodies were used to detect the proteins.

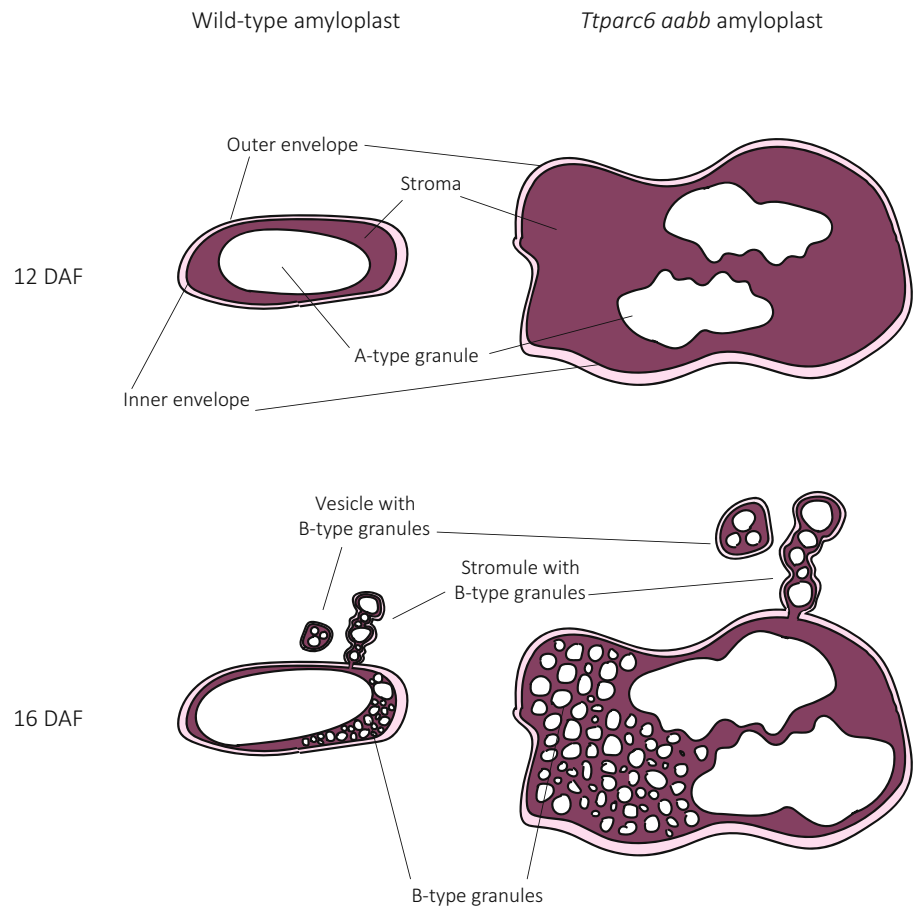


Fig. 8 Model of amyoplast and starch granule structures in wild-type and the *Ttparc6* double mutant of wheat during endosperm development. DAF, day after flowering.

Ttparc6 amyoplasts may explain the altered morphology of the A-type granules (Fig. 3g–p).

Correct amyoplast size appears to also be important for establishing the proper ratio of A and B-type granule numbers. We observed that increased stromal volume in amyoplasts is associated with greater numbers of starch granules in each amyoplast (Fig. 8). In the mutant, we identified many examples of amyoplasts containing multiple A-type granules, which were not observed in the wild-type (Fig. 6). Also, although the size of both A- and B-type granules was increased in the mutant, the total number of starch granules per milligram purified starch was the same as the wild-type (Fig. 3f), which can only be explained by a large relative increase in the number of the smaller B-type granules. This increase in relative number, together with the larger size of individual B-type granules, likely contributed to the higher B-type granule content (as % volume) in *Ttparc6* mutants compared with the wild-type controls (Fig. 3e).

Previously, different models have been proposed regarding the compartmentalisation of B-type granules. It was suggested that B-type granules were initiated and contained in amyoplast stromules (Parker, 1985; Langeveld *et al.*, 2000), or in separate vesicle-like structures (Buttrose, 1960). Our analysis of amyoplast ultrastructure in addition to live-cell imaging of amyoplasts revealed B-type granules in both amyoplast stromules and separate vesicle-like amyoplasts at 16 DAF, in both wild-type and

Ttparc6 double mutants (Figs 6, 8). In addition, we saw B-type granules within the main compartment that contained the A-type granules in both genotypes (Figs 6, 8). The occurrence of these different features in wheat supports the hypothesis that stromule formation is an intermediate state of amyoplasts containing B-type granules budding from existing amyoplasts that contain A-type granules, which was recently proposed from similar observations in barley (Matsushima & Hisano, 2019). This is also consistent with early observations that in wheat endosperm, plastid protrusions tended to be short-lived (Bechtel & Wilson, 2003). Our results therefore advance the current models of starch granule formation in wheat by demonstrating that number and size of both A- and B-type starch granules is dependent on amyoplast size and accessible stromal volume (Fig. 8). While these discoveries are specific to the bimodal type of starch granules that is unique to the Triticeae, they also highlight possible common features with other species. In *Arabidopsis* plastid division mutants, the number of starch granules in the enlarged chloroplasts increases corresponding to the increase in stromal volume such that the number of granules per stromal volume remains similar to the wild-type, and granule size is unaffected (Crumpton-Taylor *et al.*, 2012; Esch *et al.*, 2022). Moreover, in rice endosperm, various abnormal amyoplast and compound granule morphologies were observed in lines with mutations or silencing in plastid division genes (FtsZ1, FtsZ2-1, PDV1, MinD, MinE

and ARC5), including large, elongated, fused or pleiomorphic amyloplasts (Yun & Kawagoe, 2009, 2010).

Furthermore, mutations in SSG4 and SSG6, two proteins suggested to be involved in regulation of amyloplast size and development, result in larger amyloplasts in the endosperm (Matsushima *et al.*, 2014, 2016; Cai *et al.*, 2022). In these mutants, the size of the compound granule and the number of the individual granulae per amyloplast was increased relative to the wild-type (Yun & Kawagoe, 2009, 2010; Matsushima *et al.*, 2014, 2016). In rice *arc5* mutants where individual granulae within the compound granules were examined, granulae were smaller than those of wild-type, and some granulae seemed to be fused (Yun & Kawagoe, 2009). Both these observations are distinct from the large, lobed granules of the wheat *parc6* mutant, suggesting that the increases in wheat granule size by increasing amyloplast size are not necessarily achieved in species-making compound granules. However, it appears that in all cases, the number of granules per plastid appears to increase with stromal volume, albeit to varying degrees depending on species.

Another common feature of the examined species is that they retain their native granule initiation types (i.e. simple vs compound) regardless of changes in plastid size. Amyloplast division mutants of rice always produced compound granules; and despite there being multiple A- and B- type starch granules per amyloplast in the wheat *Ttparc6* double mutants, these granules did not fuse or form compound-type starch granules. The formation of compound or bimodal-type starch granules is thus independent from amyloplast size and starch granule number. It was proposed that the formation of compound-type starch granules in rice is potentially dependent on amyloplast subcompartmentalisation (Yun & Kawagoe, 2010). While its nature is not fully understood, the presence of such compartmentalisation may be more important than amyloplast size for determining different granule types.

PARC6 in wheat may complement ARC6 deficiency

In Arabidopsis, lack of PARC6 causes diverse plastid morphology phenotypes among different epidermal cell types, which are different and more complex than the phenotype observed in mesophyll cells, where the plastids are consistently increased in size and fewer in number (Ishikawa *et al.*, 2020). Since *Ttparc6* mutants had increased plastid size in both leaves and endosperm, PARC6 appears to be a common element in plastid division in the organs in wheat. However, in strong contrast to the *Ttparc6* double mutants, the *Ttarc6* double mutant had no discernible changes in the size of leaf mesophyll chloroplasts and also had normal starch granule size distribution in the endosperm (Figs S2b,c, S8a). This was surprising since in Arabidopsis, the lack of ARC6 causes very strong increases in plastid size, both in leaves and root columella cells (Robertson *et al.*, 1995; Glynn *et al.*, 2008). The mutations in the *Ttarc6* double mutants led to premature stop codons in the coding sequence of both A and B- homeologs, just after the transmembrane domain (Figs S2a, S9a). If these mutations do not fully knockout protein production, they would at least delete the C-terminal region necessary

for interaction with PDV2 (Wang *et al.*, 2017). In Arabidopsis, the deletion of this C-terminal region (like in AtARC6ΔIMS; Fig. S9a) greatly reduced ARC6 function and could only partially rescue the plastid division phenotype of *arc6* (Glynn *et al.*, 2008). Localisation and co-immunoprecipitation experiments in *N. benthamiana* indicated that *TaARC6* localises to the chloroplast envelope and can interact with *TaPDV2*, but not with either of the PDV1 paralogs in wheat (*TaPDV1-1* and *TaPDV1-2*) (Fig. 7). By contrast, *TaPARC6* could interact with *TaPDV1-1*, as well as weakly with *TaPDV1-2* and *TaPDV2*. It is possible that in wheat, the ability of PARC6 to interact with *TaPDV2* as well as *TaPDV1-1* and *TaPDV1-2* allows it to compensate for a loss of ARC6 function, which could explain the lack of plastid division phenotype in *Ttarc6* mutants.

Despite the potential overlap in interactions, it is likely that *TaPARC6* and *TaARC6* retain distinct functions, as reported in Arabidopsis (Zhang *et al.*, 2009, 2016; Sun *et al.*, 2023). The two proteins showed different subcellular localisations: *TaPARC6* formed distinct puncta at the chloroplast envelope, similar to those reported previously for the Arabidopsis ortholog (Glynn *et al.*, 2009; Ishikawa *et al.*, 2020; Fig. 7a–c). *TaARC6*, by contrast, appeared to be homogeneously distributed in the chloroplast envelope (Fig. 7d–f). Separate functions of PARC6 and ARC6 in the wheat endosperm are supported by their different temporal patterns of gene expression: *TtPARC6* expression is highest during early endosperm development (6 DPA) and lowest during late developmental stages (20 and 30 DPA) (Fig. S8d,e; Chen *et al.*, 2022b). For *TtARC6* however, expression in the endosperm is not only about tenfold higher than that of *TtPARC6*, but also peaks at c. 15 DPA, which coincides with B-type granule initiation (Fig. S8b,c). Diverse temporal expression patterns were also observed for *TtPDV* paralogs. Interestingly, while expression of *TtPDV1-2-A1* and *TtPDV1-2-B1* in the developing endosperm mimics the patterns of *TtPARC6*, expression patterns of *TtPDV1-1-A1* and *TtPDV1-1-B1* differed from each other and from *TtPARC6*. *TtPDV1-1-A1* and *TtPDV2-A1* had similar expression patterns to *TtARC6* (Fig. S8f–j). The apparently diverse functions of these PDV paralogs in grasses may be an interesting line of future investigation. Further work is also required to determine whether there are mechanistic differences in the function of PARC6 and other plastid division components between the leaves and endosperm, as well as in their regulation. For example, it was recently shown that the interaction between AtPARC6 and AtPDV1 is regulated by light, through redox and magnesium (Sun *et al.*, 2023). However, in endosperm amyloplasts of wheat, light is unlikely to be one of the factors promoting interaction of PARC6 and PDV1.

PARC6 is a novel gene target for modifying wheat starch

Mutation of *PARC6* enabled for the first time, to our knowledge, production of larger starch granules in wheat endosperm. Several benefits of wheat starch with large granule size can be predicted: They include, for example, better milling efficiency, novel functional starch properties and enhanced nutritional properties (Lindeboom *et al.*, 2004; Dhital *et al.*, 2010; Li *et al.*, 2019; Chen

et al., 2021). In addition, high B-type granule content is associated with better pasta quality (Soh *et al.*, 2006). Therefore, *PARC6* can be a novel genetic target for modifying starch granule size in wheat. While the feasibility of this will require further field testing, it is promising that under our growth conditions, the *Ttparc6* mutant was not different to the wild-type in terms of plant growth and development, photosynthetic efficiency, grain size and yield and starch content (Figs 1, 2, S3, S4). This contrasts with the rice *parc6* mutant which had slight reductions in plant growth and grain weight (Kamau *et al.*, 2015). Interestingly, all changes in starch granule morphology in the *Ttparc6* double mutants were less severe in the single mutants, and this dosage effect can be exploited to achieve a range of different starch granule sizes.

Acknowledgements

The authors thank the John Innes Centre (JIC) Horticultural Services for providing growth facilities and maintenance of plant material, JIC Bioimaging for providing access to microscopes, JIC Crop Transformation for providing transformation resources and expertise, the JIC Genotyping platform for providing DNA extraction and KASP genotyping, and Alexander Watson-Lazowski (Harper Adams University) and Richard Vath (University of Cambridge) for helpful advice on the gas-exchange experiments. This work was funded through a Leverhulme Trust Research Project grant RPG-2019-095 (to DS and AMS), a John Innes Foundation (JIF) Chris J. Leaver Fellowship (to DS), a JIF Rotation Ph.D. studentship (to RM) and BBSRC Institute Strategic Programme grants BBS/E/J/000PR9790 and BBS/E/J/000PR9799 (to the John Innes Centre).









Competing interests

LE and DS are coinventors on a patent for using *PARC6* to alter starch granule morphology. We have no other conflicts of interest to declare.

Author contributions

LE, AMS and DS conceived and designed the experiments. LE, QYN, JEB, SH and MAS performed the experiments. LE, QYN and RM analysed the data. LE and DS wrote the paper (with input from all authors).

ORCID

J. Elaine Barclay  <https://orcid.org/0000-0001-8560-410X>
Lara Esch  <https://orcid.org/0000-0003-2049-1882>
Sadiye Hayta  <https://orcid.org/0000-0003-2920-4720>
Rose McNelly  <https://orcid.org/0000-0002-5313-7380>
Qi Yang Ngai  <https://orcid.org/0000-0002-8154-7272>
David Seung  <https://orcid.org/0000-0003-3905-3647>
Mark A. Smedley  <https://orcid.org/0000-0002-6162-4795>
Alison M. Smith  <https://orcid.org/0000-0001-6927-9650>

Data availability

The data that support the findings of this study are available in the main figures and [Supporting Information](#).

References

- Appels R, Eversole K, Feuillet C, Keller B, Rogers J, Stein N, Pozniak CJ, Choulet F, Distelfeld A, Poland J *et al.* 2018. Shifting the limits in wheat research and breeding using a fully annotated reference genome. *Science* **361**: eaar7191.
- Bechtel DB, Wilson JD. 2003. Amyloplast formation and starch granule development in hard red winter wheat. *Cereal Chemistry* **80**: 175–183.
- Bechtel DB, Zayas I, Kaleikau L, Pomeranz Y. 1990. Size-distribution of wheat starch granules during endosperm development. *Cereal Chemistry* **67**: 59–63.
- Buttrose MS. 1960. Submicroscopic development and structure of starch granules in cereal endosperms. *Journal of Ultrastructure Research* **4**: 231–257.
- Cai Y, Chen H, Xiao N, Wu Y, Yu L, Chen Z, Liu J, Shi W, Pan C, Li Y *et al.* 2022. Substandard starch grain4 may function in amyloplast development by influencing starch and lipid metabolism in rice endosperm. *Journal of Plant Physiology* **270**: 153638.
- Carciofi M, Blennow A, Jensen SL, Shaik SS, Henriksen A, Buléon A, Holm PB, Hebelstrup KH. 2012. Concerted suppression of all starch branching enzyme genes in barley produces amylose-only starch granules. *BMC Plant Biology* **12**: 1–16.
- Chen C, MacCready JS, Ducat DC, Osteryoung KW. 2018. The molecular machinery of chloroplast division. *Plant Physiology* **176**: 138–151.
- Chen J, Chen Y, Watson-Lazowski A, Hawkins E, Barclay JE, Fahy B, Denley-Bowers R, Corbin K, Warren FJ, Blennow A *et al.* 2022a. Contrasting roles of the wheat MRC in promoting starch granule initiation in leaves and repressing the onset of B-type granule initiation in the endosperm. *bioRxiv*. doi: [10.1101/2022.10.07.511297](https://doi.org/10.1101/2022.10.07.511297).
- Chen J, Hawkins E, Seung D. 2021. Towards targeted starch modification in plants. *Current Opinion in Plant Biology* **60**: 102013.
- Chen J, Watson-Lazowski A, Vickers M, Seung D. 2022b. Gene expression profile of the developing endosperm in durum wheat provides insight into starch biosynthesis. *bioRxiv*. doi: [10.1101/2022.10.21.513215](https://doi.org/10.1101/2022.10.21.513215).
- Chia T, Chirico M, King R, Ramirez-Gonzalez R, Saccomanno B, Seung D, Simmonds J, Trick M, Uauy C, Verhoeven T *et al.* 2020. A carbohydrate-binding protein, B-GRANULE CONTENT 1, influences starch granule size distribution in a dose-dependent manner in polyploid wheat. *Journal of Experimental Botany* **71**: 105–115.
- Crumpton-Taylor M, Grandison S, Png KMY, Bushby AJ, Smith AM. 2012. Control of starch granule numbers in Arabidopsis chloroplasts. *Plant Physiology* **158**: 905–916.
- De Pater S, Caspers M, Kottenhagen M, Meima H, Ter Stege R, De Vetten N. 2006. Manipulation of starch granule size distribution in potato tubers by modulation of plastid division. *Plant Biotechnology Journal* **4**: 123–134.
- Dhital S, Shrestha AK, Gidley MJ. 2010. Relationship between granule size and *in vitro* digestibility of maize and potato starches. *Carbohydrate Polymers* **82**: 480–488.
- Esch L, Ngai QY, Barclay JE, Seung D. 2022. AtFZL is required for correct starch granule morphology in Arabidopsis chloroplasts. *bioRxiv*. doi: [10.1101/2022.10.20.512996](https://doi.org/10.1101/2022.10.20.512996).
- Evers AD. 1971. Scanning electron microscopy of wheat starch III. Granule development in the endosperm. *Starch – Stärke* **23**: 157–162.
- Fahy B, Gonzalez O, Savva GM, Ahn-Jarvis JH, Warren FJ, Dunn J, Lovegrove A, Hazard BA. 2022. Loss of starch synthase IIIa changes starch molecular structure and granule morphology in grains of hexaploid bread wheat. *Scientific Reports* **12**: 1–14.
- Glynn JM, Froehlich JE, Osteryoung KW. 2008. Arabidopsis ARC6 coordinates the division machineries of the inner and outer chloroplast membranes through interaction with PDV2 in the intermembrane space. *Plant Cell* **20**: 2460–2470.
- Glynn JM, Yang Y, Vitha S, Schmitz AJ, Hemmes M, Miyagishima SY, Osteryoung KW. 2009. *PARC6*, a novel chloroplast division factor, influences

- FtsZ assembly and is required for recruitment of PDV1 during chloroplast division in Arabidopsis. *The Plant Journal* 59: 700–711.
- Hanson MR, Conklin PL. 2020. Stromules, functional extensions of plastids within the plant cell. *Current Opinion in Plant Biology* 58: 25–32.
- Hawkins E, Chen J, Watson-Lazowski A, Ahn-Jarvis J, Barclay JE, Fahy B, Hartley M, Warren FJ, Seung D. 2021. STARCH SYNTHASE 4 is required for normal starch granule initiation in amyloplasts of wheat endosperm. *New Phytologist* 230: 2371–2386.
- Hayta S, Smedley MA, Clarke M, Forner M, Harwood WA. 2021. An efficient *Agrobacterium*-mediated transformation protocol for hexaploid and tetraploid wheat. *Current Protocols* 1: e58.
- Howard T, Rejab NA, Griffiths S, Leigh F, Leverington-Waite M, Simmonds J, Uauy C, Trafford K. 2011. Identification of a major QTL controlling the content of B-type starch granules in *Aegilops*. *Journal of Experimental Botany* 62: 2217–2228.
- Ishikawa H, Yasuzawa M, Koike N, Sanjaya A, Moriyama S, Nishizawa A, Matsuoka K, Sasaki S, Kazama Y, Hayashi Y *et al.* 2020. Arabidopsis PARC6 is critical for plastid morphogenesis in pavement, trichome, and guard cells in leaf epidermis. *Frontiers in Plant Science* 10: 1–19.
- Jarvis P, López-Juez E. 2013. Biogenesis and homeostasis of chloroplasts and other plastids. *Nature Reviews. Molecular Cell Biology* 14: 787–802.
- Johnson CB, Tang LK, Smith AG, Ravichandran A, Luo Z, Vitha S, Holzenburg A. 2013. Single particle tracking analysis of the chloroplast division protein ftsz anchoring to the inner envelope membrane. *Microscopy and Microanalysis* 19: 507–512.
- Kamau PK, Sano S, Takami T, Matsushima R, Maekawa M, Sakamoto W. 2015. A mutation in GIANT CHLOROPLAST encoding a PARC6 homolog affects spikelet fertility in rice. *Plant & Cell Physiology* 56: 977–991.
- Koksharova OA, Wolk CP. 2002. A novel gene that bears a DnaJ motif influences cyanobacterial cell division. *Journal of Bacteriology* 184: 5524–5528.
- Krasileva KV, Vasquez-Gross HA, Howell T, Bailey P, Paraiso F, Clissold L, Simmonds J, Ramirez-Gonzalez RH, Wang X, Borrill P *et al.* 2017. Uncovering hidden variation in polyploid wheat. *Proceedings of the National Academy of Sciences, USA* 114: E913–E921.
- Langeveld SM, van Wijk R, Kijne JW, de Pater S. 2000. B-type granule containing protrusions and interconnections between amyloplasts in developing wheat endosperm revealed by transmission electron microscopy and GFP expression. *Journal of Experimental Botany* 349: 1357–1361.
- Li H, Gidley MJ, Dhital S. 2019. High-amylose starches to bridge the “fiber gap”: development, structure, and nutritional functionality. *Comprehensive Reviews in Food Science and Food Safety* 18: 362–379.
- Lindeboom N, Chang PR, Tyler RT. 2004. Analytical, biochemical and physicochemical aspects of starch granule size, with emphasis on small granule starches: a review. *Starch – Staerke* 56: 89–99.
- Maccaferri M, Harris NS, Twardziok SO, Pasam RK, Gundlach H, Spannagl M, Ormanbekova D, Lux T, Prade VM, Milner SG *et al.* 2019. Durum wheat genome highlights past domestication signatures and future improvement targets. *Nature Genetics* 51: 885–895.
- Marbouty M, Saguez C, Cassier-Chauvat C, Chauvat F. 2009. ZipN, an FtsA-like orchestrator of divisome assembly in the model cyanobacterium *Synechocystis* PCC6803. *Molecular Microbiology* 74: 409–420.
- Matsushima R, Hisano H. 2019. Imaging amyloplasts in the developing endosperm of barley and rice. *Scientific Reports* 9: 1–10.
- Matsushima R, Maekawa M, Kusano M, Kondo H, Fujita N, Kawagoe Y, Sakamoto W. 2014. Amyloplast-localized SUBSTANDARD STARCH GRAIN4 protein influences the size of starch grains in rice endosperm. *Plant Physiology* 164: 623–636.
- Matsushima R, Maekawa M, Kusano M, Tomita K, Kondo H, Nishimura H, Crofts N, Fujita N, Sakamoto W. 2016. Amyloplast membrane protein SUBSTANDARD STARCH GRAIN6 controls starch grain size in rice endosperm. *Plant Physiology* 170: 1445–1459.
- Matsushima R, Yamashita J, Kariyama S, Enomoto T, Sakamoto W. 2013. A phylogenetic re-evaluation of morphological variations of starch grains among Poaceae species. *Journal of Applied Glycoscience* 60: 37–44.
- Mazouni K, Domain F, Cassier-Chauvat C, Chauvat F. 2004. Molecular analysis of the key cytokinetic components of cyanobacteria: FtsZ, ZipN and MinCDE. *Molecular Microbiology* 52: 1145–1158.
- Mingo-Castel AM, Pelacho AM, de Felipe MR. 1991. Amyloplast division in kinetin induced potato tubers. *Plant Science* 73: 211–217.
- Miyagishima S. 2011. Mechanism of plastid division: from a bacterium to an organelle. *Plant Physiology* 155: 1533–1544.
- Miyagishima SY, Froehlich JE, Osteryoung KW. 2006. PDV1 and PDV2 mediate recruitment of the dynamin-related protein ARC5 to the plastid division site. *Plant Cell* 18: 2517–2530.
- Osteryoung KW, Pyke KA. 2014. Division and dynamic morphology of plastids. *Annual Review of Plant Biology* 65: 443–472.
- Parker ML. 1985. The relationship between A-type and B-type granules in the developing endosperm of wheat. *Journal of Cereal Science* 3: 271–278.
- Robertson EJ, Pyke KA, Leech RM. 1995. arc6, an extreme chloroplast division mutant of Arabidopsis also alters proplastid proliferation and morphology in shoot and root apices. *Journal of Cell Science* 108: 2937–2944.
- Sakamoto W, Miyagishima S, Jarvis P. 2008. Chloroplast biogenesis: control of plastid development, protein import, division and inheritance. *The Arabidopsis Book* 6: e0110.
- Soh HN, Sissons MJ, Turner MA. 2006. Effect of starch granule size distribution and elevated amylose content on durum dough rheology and spaghetti cooking quality. *Cereal Chemistry* 83: 513–519.
- Stokes KD, McAndrew RS, Figueroa R, Vitha S, Osteryoung KW. 2000. Chloroplast division and morphology are differentially affected by overexpression of FtsZ1 and FtsZ2 genes in Arabidopsis. *Plant Physiology* 124: 1668–1677.
- Streb S, Delatte T, Umhang M, Eicke S, Schorderet M, Reinhardt D, Zeeman SC. 2008. Starch granule biosynthesis in Arabidopsis is abolished by removal of all debranching enzymes but restored by the subsequent removal of an endoamylase. *Plant Cell* 20: 3448–3466.
- Sun Q, Cao X, Liu S, An C, Hu J, Wnag Y, Qiao M, Gao T, Cheng W, Zhang Y *et al.* 2023. Structural and functional insights into the chloroplast division site regulators PARC6 and PDV1 in the intermembrane space. *Proceedings of the National Academy of Sciences, USA* 120: 1–11.
- Sun T, Yuan H, Cao H, Yazdani M, Tadmor Y, Li L. 2018. Carotenoid metabolism in plants: the role of plastids. *Molecular Plant* 11: 58–74.
- Vitha S, Froehlich JE, Koksharova O, Pyke KA, Van Erp H, Osteryoung KW. 2003. ARC6 is a J-domain plastid division protein and an evolutionary descendant of the cyanobacterial cell division protein Ftn2. *Plant Cell* 15: 1918–1933.
- Wang W, Li J, Sun Q, Yu X, Zhang W, Jia N, An C, Li Y, Dong Y, Han F *et al.* 2017. Structural insights into the coordination of plastid division by the ARC6-PDV2 complex. *Nature Plants* 3: 1–9.
- Washington JM, Box A, Karakousis A, Barr AR. 2000. Developing waxy barley cultivars for food, feed and malt. *Barley Genetics* VIII: 303–306.
- Yoshida Y, Miyagishima SY, Kuroiwa H, Kuroiwa T. 2012. The plastid-dividing machinery: formation, constriction and fission. *Current Opinion in Plant Biology* 15: 714–721.
- Yoshida Y, Mogi Y. 2019. How do plastids and mitochondria divide? *Microscopy* 68: 45–56.
- Yun MS, Kawagoe Y. 2009. Amyloplast division progresses simultaneously at multiple sites in the endosperm of rice. *Plant & Cell Physiology* 50: 1617–1626.
- Yun MS, Kawagoe Y. 2010. Septum formation in amyloplasts produces compound granules in the rice endosperm and is regulated by plastid division proteins. *Plant & Cell Physiology* 51: 1469–1479.
- Zhang M, Chen C, Froehlich JE, Terbush AD, Osteryoung KW. 2016. Roles of Arabidopsis PARC6 in coordination of the chloroplast division complex and negative regulation of FtsZ Assembly. *Plant Physiology* 170: 250–262.
- Zhang M, Hu Y, Jia J, Li D, Zhang R, Gao H, He Y. 2009. CDP1, a novel component of chloroplast division site positioning system in Arabidopsis. *Cell Research* 19: 877–886.

Supporting Information

Additional Supporting Information may be found online in the Supporting Information section at the end of the article.

Fig. S1 Molecular phylogenetic analysis of *ARC6* and *PARC6* gene families.

Fig. S2 *TaARC6* gene models and chloroplast morphology of the *Ttarc6* mutant.

Fig. S3 Growth and seed phenotype of *Ttparc6* single homeolog mutants.

Fig. S4 Photosynthesis parameters of *Ttparc6* mutant plants.

Fig. S5 Size distribution of purified starch granules from mature grains of the *Ttparc6* single mutants.

Fig. S6 Plant growth, grain morphology and starch phenotypes of the *Ttparc6* mutant expressing the cTPmCherry amyloplast marker.

Fig. S7 Analysis of properties of *TtPARC6*-deficient *Triticum turgidum* starch.

Fig. S8 Size distribution of starch granules of the *Ttarc6* mutant and *TtARC6* and *TtPARC6* expression patterns during endosperm development.

Fig. S9 Molecular phylogenetic analysis of *PDV1* and *PDV2* gene families and *ARC6* mutant protein alignment.

Methods S1 Phylogenetic analysis and gene models.

Methods S2 Cloning and construct assembly.

Methods S3 Transient transformation of *Nicotiana benthamiana*.

Methods S4 Gas exchange.

Methods S5 Starch purification, scanning electron microscopy and polarised light microscopy.

Methods S6 Total starch quantification, starch composition and amylopectin structure.

Methods S7 Analysis of chloroplast morphology.

Methods S8 Microscopic analysis of amyloplast morphology in developing grain.

Table S1 KASP-markers for *Ttparc6* and *Ttarc6* genotyping.

Table S2 Codon optimised DNA sequences of *TaPARC1-A1*, *TaARC6-A1*, *TaPDV1-1-A1*, *TaPDV1-2-A1* and *TaPDV2-A1*.

Please note: Wiley is not responsible for the content or functionality of any Supporting Information supplied by the authors. Any queries (other than missing material) should be directed to the *New Phytologist* Central Office.